Numerical simulation of flow pattern around submerged vanes placed in front of intake at 180º bend

Massumeh Rostamabadi[1], S. Ali Akbar Salehi Neyshabouri[2], &Hossein Montaseri

[1]Department of civil engineering, Buinzahra Branch, Islamic Azad University (I.A.U), Bouinzahra, Iran.
[2]Water Engineering Research Institute, University of Tarbiat Modares, Tehran, Iran.
[3]Department of civil engineering, University of Yassoj, Yassoj, Iran.

E-mail: [1]Rostamimass@yahoo.com
E-mail:[2]salehi@modares.ac.ir
E-mail: [3]Hmontaseri@gmail.com

Abstract

Three dimensional model FLUENT is used to simulate and analysis of flow pattern around submerged vanes placed in front of the diversion entrance, located at 115° position with diversion angles of 45 degree, in 180 degree bend with rigid bed. Computations are performed using Reynolds Stress Model. Comparison of the predicted velocity field with laboratory measurements indicates that the model captures experimental trend with reasonable accuracy. The numerical model are used to elucidate the complex 3D flow field in front of intake, including flow dividing, zones of separation and secondary flow around vanes.

Introduction

Submerged vanes are plane structures with small height-length ratio ranging from 0.1-0.5, placed on river bed with an angle to the approach flow which cause secondary flow. The height is normally set at 0.2-0.4 times of the local water depth. As the approach flow attacks a vane, a high pressure zone and a low pressure zone form at the upstream and downstream faces of the vane, respectively. The pressure differential across a vane induces a current over the top of the vane, which is carried downstream as helicoidally vortex and is responsible for changes in the near bed velocity, shear stresses and hence the topography in the vicinity of the vane. So the vanes are used to reduce sediment entrainment from water intake structures, protect against bank erosion and increase navigation depth.

In recent decades, there has been an increasing trend in the use of submerged vanes as sediment management devices because of their smaller dimensions and less structural cost as opposed to the traditional sediment control structures.

The most detailed recent studies describing the flow field and dimensions of vanes are attributed to Odgaard and co-workers at the university of Iowa hydraulic research. Odgaard and Spoljaric (1986) presented a simplified theoretical and experimental analysis of flow in a straight rectangular channel and proposed the optimum vane height, length and angle of attack with flow. A laboratory study that examines the effectiveness of submerged vanes for the control of erosion in strongly curved narrow channel bend was performed by Voisin and Townsend (2002). They concluded that submerged vanes affectively stabilize channel bend erosion by reducing the net sediment loss through channel. The flow field around submerged vanes is documented in the literature based on a few laboratory experiments done by Marelius and Sinha (1998), Soon-keat et al (2005) and a numerical model study by Marelius and Sinha (2000) in straight rectangular channel. Barkdol (1999) through study on a laboratory experiments in straight channel shows that a pattern of submerged vanes placed at the diversion entrance admits negligible rate of bed sediment entry into the diversion when the ratio of unit discharge in the diversion to unit discharge in the main channel is less than 0.2.

Although the above-mentioned studies provided part of needed insight into the physics of vanes function, they did not address detailed descriptions of flow pattern around vanes placed in front of intake in the bend. The three-dimensional flow field around vanes in front of intake at curved channel is complex duo to secondary flow and interaction between intake, bend and vanes. It might be necessary to further study about the flow physics to ensure the desired performance of the submerged vanes.

Numerical simulation supplement experimental studies in understanding the complex flow field especially where the laboratory experiments are either impossible because of the complexity of the flow and large degree of variability or taken with uncertainty.

The objectives of this paper are numerical simulation of flow pattern around a spatial arrangement of submerged vanes (figure 1 and 2) placed in front of the intake entrance in curved channel (r/b=4.33) with 180 degree bend, and hydrodynamic analysis of the interaction between vanes system, intake and bend flow pattern.

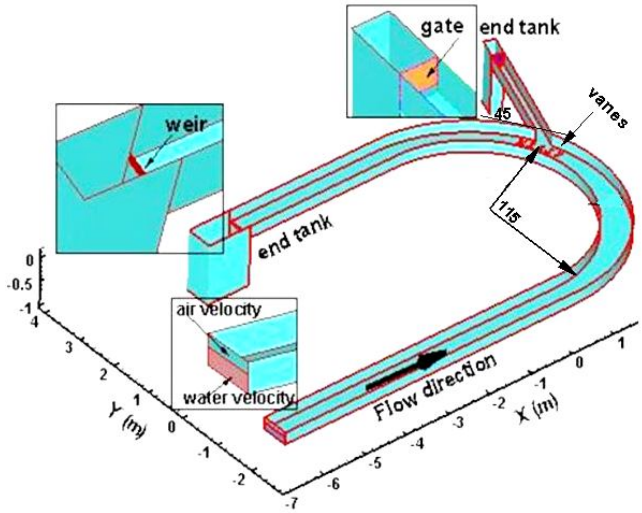

Figure 1: 3-D view of simulation flume

Computational Domain

The computational domain consists of three parts; main channel, intake channel and submerged vanes. The main channel has a rectangular cross section measuring 0.6 m wide by 0.6 m deep and comprised three sections: (i) an initial straight section of 7 m length, (ii) 180° bend section with central radius of 2.6 m, and (iii) a final straight section of 3.5 m length. The intake channel is positioned at 115° with rectangular cross section (0.25 m width, 0.3 m depth) with 2.5 m length. The diversion discharge is controlled by a sluice gate at the end of the intake channel as shown in figure 1.

Two rows of submerged vanes initiating from 105° position with 0.003 m thick, 0.035 m height and 0.105 m length with angle of 20 degree to the main flow direction are placed on channel bed. The transverse distance from the channel outer bank to the vane centerline (δ_b) and between rows of vanes is 0.1 m. The stream wise spacing (δ_s) between vanes is 0.1 m (figure 2).

A two phase domain containing water with 0.15 m depth (h0) initially in channel with a region of air at the top is solved using the multiphase flow model (VOF). The depth of air should be large enough to avoid any effect from the boundary condition at the top of the domain. If the ratio of initial depth of air to the initial depth of water is one-third or larger, there is no effect from the boundary at the top of the domain (Tarek and Imran, 2004). In this paper due to the effect of bend and intake on variation of water surface, this ratio is set to two-third. So the channel with 0.25 m depth is simulated. In order to be consistent with the experimental model, two reservoirs with 1 m depth and length, at the end of the main and intake channel have been set for falling flow.

Grid layout

The law of the wall is used to calculate the bottom shear stress. The size of the cells adjacent to solid boundaries is chosen to satisfy the limits of wall unit distance $11.25 < z^+ < 30$, where: $z^+ = \frac{\rho u_* z_p}{\mu}$; ρ = fluid density; u_* = shear velocity; μ = dynamic viscosity and

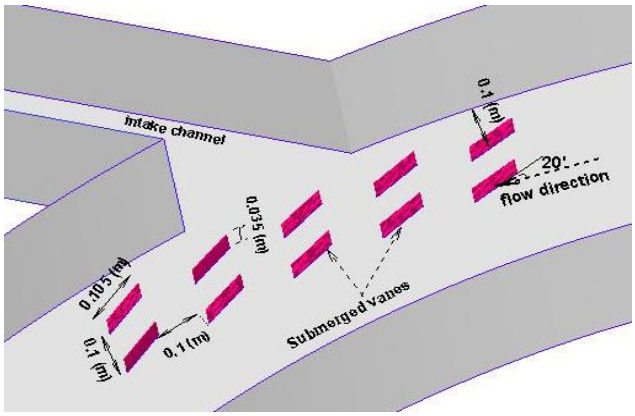

Figure 2: Arrangement of vanes

z_p = distance from cell adjacent to solid boundary. Grid size should be fine near the wall and air-water interface to capture the small variation of the free surface. 150,000 nodes are generated using Gambit 2. A 3D view of a computational mesh is shown in figure 3.

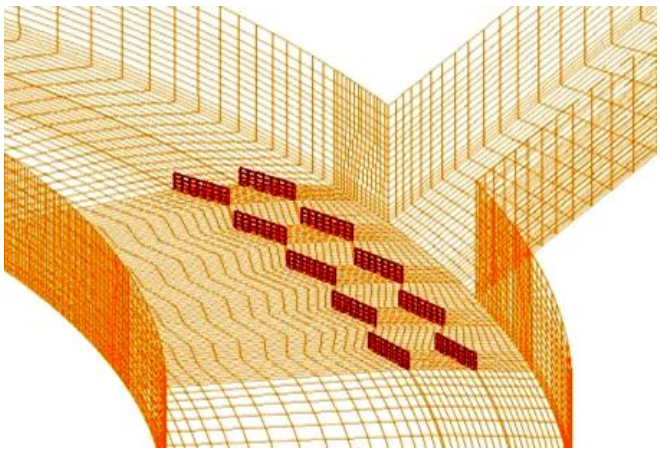

Figure 3: computational grid

Model description

A robust 3D computational fluid dynamics (CFD) solver FLUENT is utilized to solve the three-dimensional Reynolds-Averaged Navier-Stokes equations.

Computations are performed using Reynolds Stress Model. The predicted velocity field is compared with experimental data (Montaseri, 2007) measured in Hydraulic Laboratory of Tarbiat Modares University. For simulation of vortex flows around submerged vanes and secondary flow at the bend, second order upwind scheme is used to discretize equations and Piso is used for coupling pressure and velocity.

In order to resolve the variation of the water surface at bend and around intake, two-phase domain is solved using VOF method. While two continuity equations are solved to account for each phase, the momentum and transport equations are shared by both phases. The continuity equation for the qth phase and Reynolds-Averaged momentum equations can be expressed as (equations 1 to 3):

$$\frac{\partial \alpha_q}{\partial t} + u_i \frac{\partial \alpha_q}{\partial x_i} = ۰ \qquad (1)$$

$$\frac{\partial}{\partial t}(\rho u_i) + \frac{\partial}{\partial x_j}(\rho u_i u_j) = -\frac{\partial P}{\partial x_i} + \frac{\partial \tau_{ij}}{\partial x_j} + \rho g_i \qquad (2)$$

$$\tau_{ij} = \left[\rho(\upsilon + \upsilon_t)\left(\frac{\partial u_i}{\partial x_j} + \frac{\partial u_j}{\partial x_i}\right)\right] - \left[\frac{۲}{۳}\rho(\upsilon_t + k)\frac{\partial u_i}{\partial x_i}\delta_{ij}\right] \qquad (3)$$

where α_q =volume fraction of the qth phase in the control volume; u_i represents velocity in the x_i direction; P=total pressure; t=time; g_i =gravitational acceleration in the i direction, $\rho = \sum \alpha_q \rho_q$ = average local density in the control volume; τ_{ij} = stress tensor; υ and υ_t = cinematic molecular and turbulent viscosity, respectively; k=turbulent kinetic energy and δ_{ij} =Kronecker delta. The volume fraction equations will not be solved for the primary phase and will be computed based on the following constraint (Fluent. Inc 2005):

$$\sum_{q=۱}^{n} \alpha_q = ۱ ; \text{ (n= number of phases)} \qquad (4)$$

The Reynolds Stress Model (RSM) provides closure of the Reynoldes-Averaged Navier-Stokes equations by solving transport equations for Reynolds stress and equation of energy dissipation rate (ε). It is considered to be superior to other models (one and two-equation) in simulating complex flows since it accounts for the effects of streamlines curvature, vorticity, circulation and rapid changes in the strain rate, but requires extensive computational effort and time. Sensitivity analysis of the numerical model to the turbulence models and grid independency was carried out for one phase simulation due to long run time of two phase model.

Figure 4 shows the comparison of the velocity magnitude of numerical model for two different turbulence models i.e. k-ε and RSM turbulence models at $\theta = 125$ degree section for five different radial distances from outer bank. Comparisons were also carried out at other sections (Rostamabadi, 2007). It is observed that the RSM predicted the velocity more accurately than k-ε. So the RSM turbulence model was selected.

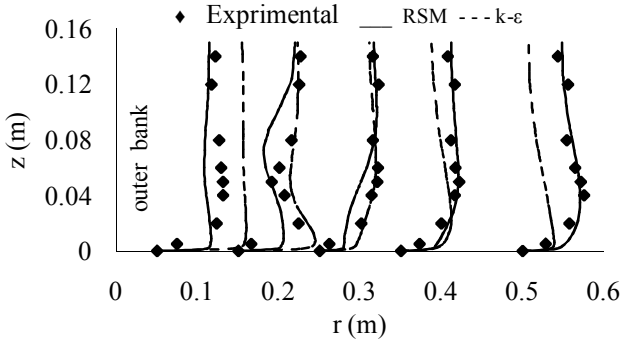

Figure 4: Comparison of numerical results for different turbulence models and experimental data (θ=125 degree).

Figure 5 shows the comparison of the numerical results for three different grid i.e. fine mesh (500,000 nodes), medium mesh (250,000 nodes) and coarse mesh (112,000 nodes) and experimental results at θ=115 degree. As shown three grids have nearly the same results and for saving of time, the coarse mesh was selected. Comparisons were also carried out at other sections (Rostamabadi, 2007). So the coarse mesh was selected and the grid with 150,000 nodes was generated for two phase simulation.

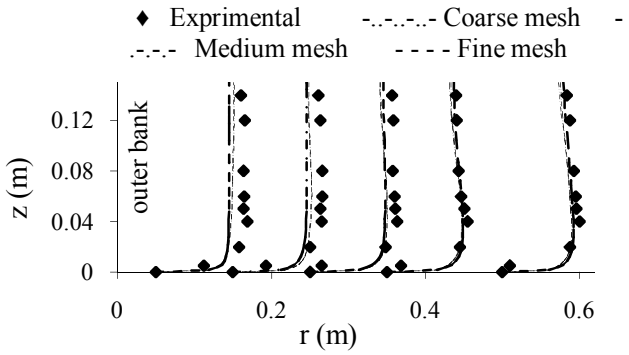

Figure 5: Comparison of numerical results for different grids and experimental data (θ=115 degree).

Depending on the nature of the flow, appropriate conditions must be specified at domain boundaries. In this paper, velocity inlet boundary condition was specified for air and water phases at the main channel inlet and turbulent intensity and hydraulic diameter were specified to compute

other variables. Pressure inlet boundary condition is used for top surface. For bed of channels and reservoirs, lateral wall of channels and submerged vanes, the wall boundary condition is used and the no-slip boundary condition is specified to set the velocity to be zero at the solid boundaries. Initial conditions VOF=1 and VOF=0 are specified for water and air phase, respectively. From t=0 (sec) (when the velocity of water phase is zero) the numerical model is run and after about t=30 (sec) reasonable convergence (residual less than 10^{-6}) obtained.

Results and discussions

Verification of numerical model

Velocity magnitude profiles predicted by numerical model at z/h0=0.8 for eight cross sections of the bend from $\theta =$ 100 degree to $\theta = 125$ degree ,and vertical distribution of velocity magnitude at $\theta = 102$ degree and $\theta = 125$ degree for five different radial distances from outer bank are compared with measured (Montaseri, 2007) velocity magnitude profiles. There is no reported data in intake channel. As shown in figure 6(a to c), good agreement is found between the experimental data and the present numerical results with mean error of average velocity at z/h0=0.8 about 3.64 %. Comparison between calculated and measured longitudinal water surface profile is shown in figure 6.d, as well which shows that computed results recover the trend of the measurements. The low and high water surface elevation are respectively associated with low and high pressure regions at the upstream and downstream corner of the entrance face of the intake.

Flow pattern

Secondary flow

The vectorial calculated secondary flow at five cross sections located at different positions of the bend is presented in figure 7. At the inlet of bend there is a unidirectional motion toward the inner bank (figure 7-a). This motion prevails due to the transverse pressure gradient and gives rise to a secondary motion cell. As the flow progress in the downstream direction, the secondary flow develops and rotation is such that fluid particles with high momentum near the surface move toward the outer bank while particles with low momentum near the bed move toward the inner bank (figure 7-b). As the flow attack vanes, the vane-induced vortices with the same direction of the main secondary flow are generated (figure 7-c). Near the intake (figure 7-d), suction of the intake drags the vortices core toward the intake; Furthermore surface flow are diverted more into the intake. Figure 7- e shows that after the intake, the vane-induced secondary flow and main secondary flow are combined into a vortex cell and decay as the flow progresses in the downstream direction.

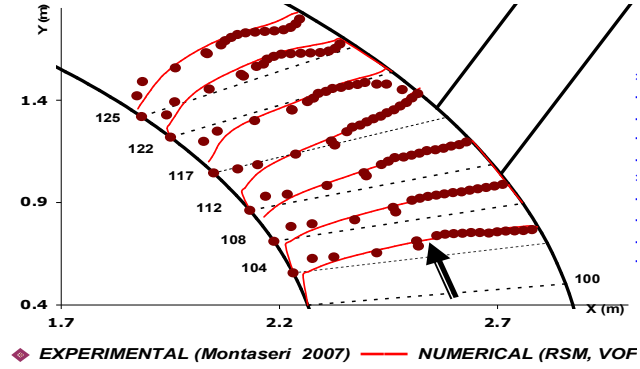

(a)

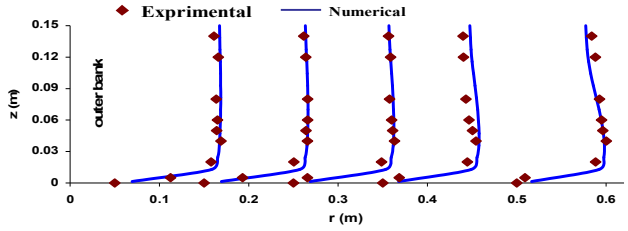

(b)

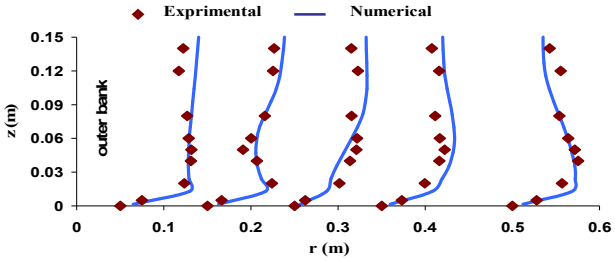

(c)

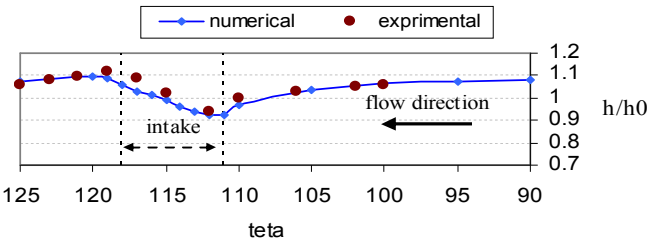

(d)

Figure 6: verification of numerical model, a: Velocity magnitude at z/h0=0.8, b: vertical distribution of velocity magnitude at $\theta = 102$ degree, c: vertical distribution of velocity magnitude at $\theta = 125$ degree, and d: longitudinal water surface profile near the outer bank.

2-D streamlines plots

Figure 8 shows 2-D streamlines plots at five horizontal planes. Theses plots elucidate the structure of the dividing stream surface, the zone of flow separation and the vanes effect on deviation of flow from intake entrance face. By comparing figures 8-a and 8-e, it is seen that, for the first half of the bend, the main secondary current of the bend (see Meselhe & Sotiropoulos, 2003 and Leschziner & Rodi, 1979) deviates surface layer toward the outer bank and near-bed layer toward the inner bank.Combination of this

vortex flow with pressure gradient cause helicoidally flow in the bend.

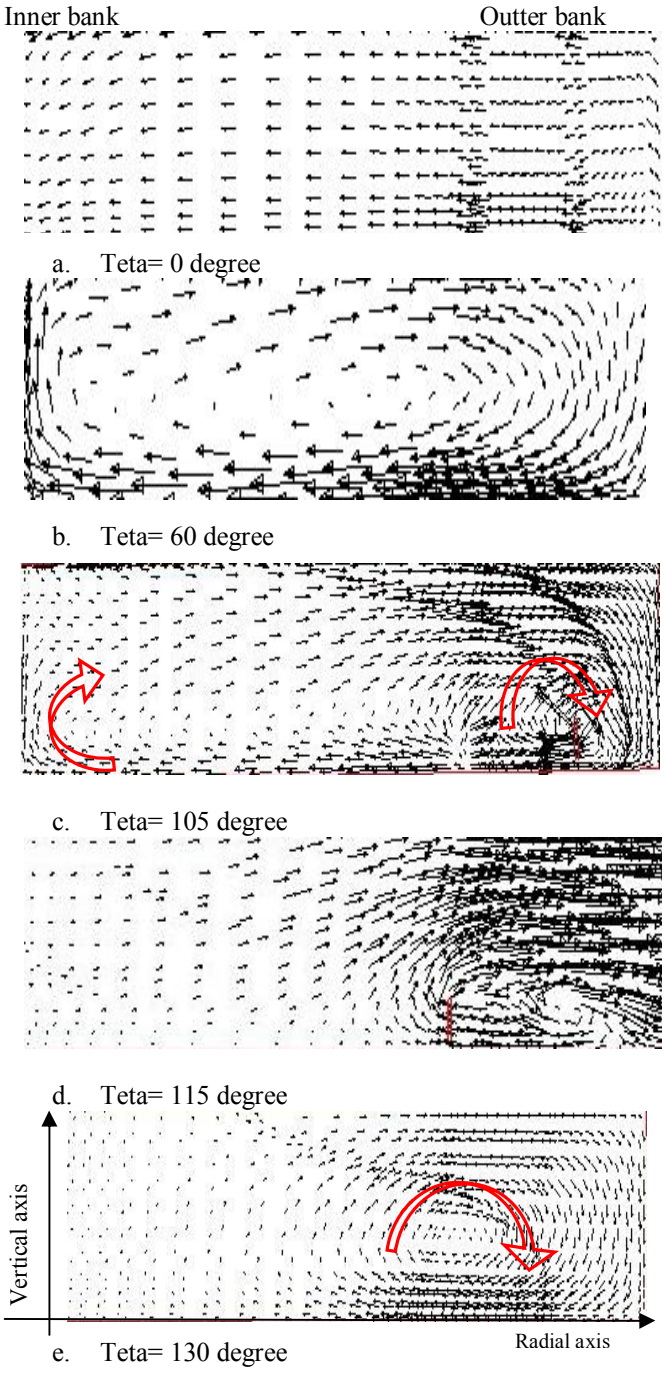

Figure 7: velocity vectors at different sections of bend

As the flow approaches the intake, it is accelerated by the suction of the branch. This causes the flow to divide so that a portion of it enters the branch channel while the reminder continues to the downstream in the main channel. The diverted flow experiences an imbalance between the transverse pressure gradient, shear and centrifugal forces that initiates a secondary flow at opposite direction of the main secondary flow denoted as intake secondary flow. The boundary surface between these two portions of flow is a curved shear layer surface, denoted as the dividing stream surface (see Neary et al, 1999).

By comparing figures 8-a to 8-e, it is seen that the dividing stream surface extends farther out in the main channel near the surface than at the bottom as opposed to the lateral intake in straight channel (see Neary et al, 1999). As the near bed flow attacks vanes, the vane-induced secondary flow deviates near-bed streamlines toward the inner wall of the main channel, and upper layer toward the outer bank and hence toward the intake. So from bottom up to the vane crest elevation, the dividing stream surface is located behind the vanes closer to the diversion bank and diversion is fed at the bed by streamlines just close to the intake surface. The same results of vanes effect on diversion of streamlines at lateral intake in straight channel have been observed by Barkdoll et al (1999) in laboratory experiments. The near bed contraction of the dividing stream surface reduces the proportion of the diversion flow from near bed. The implication of these flow patterns on sediment transport is that, because of a small portion of the near-bed flow is diverted, the branch channel will receive small amount of bed load.

The near bed streamlines show that there are streamlines in the main channel that impinge on the outer bank near the downstream corner of the intake entrance at higher elevation and are deflected downward toward the bed. As they attack to the last vanes, they deviate toward the inner wall of the main channel. The space between theses streamlines and flow dividing stream surface, is a low velocity zone near the bed just off the downstream corner of the intake, as opposed to saddle stagnation zone at diversion without vanes (see Neary et al, 1999). This low velocity zone shown in figure 8-b can be a probable sedimentation zone.

By comparing figures 8-a and 8-e, it is seen that because of higher momentum of surface flow compared to the near-bed flow, the separation zone in front of upstream bank of intake channel being narrower at the bottom than at the surface.

Strength of secondary flow

Figure 9 shows the interaction between the vane-induced and intake secondary flow on the strength of main secondary flow computed by equation 5 (Daily & Harleman, 1966):

$$\omega_\theta = \frac{1}{2}\left(\frac{\partial v_r}{\partial z} - \frac{\partial v_z}{\partial r}\right) \qquad (5)$$

Where ω_θ = tangential vorticity; v_r = radial velocity component and v_z = z-axis velocity component. It is seen that the longitudinal secondary flow has the maximum strength at 60° section for the first half of the bend and the

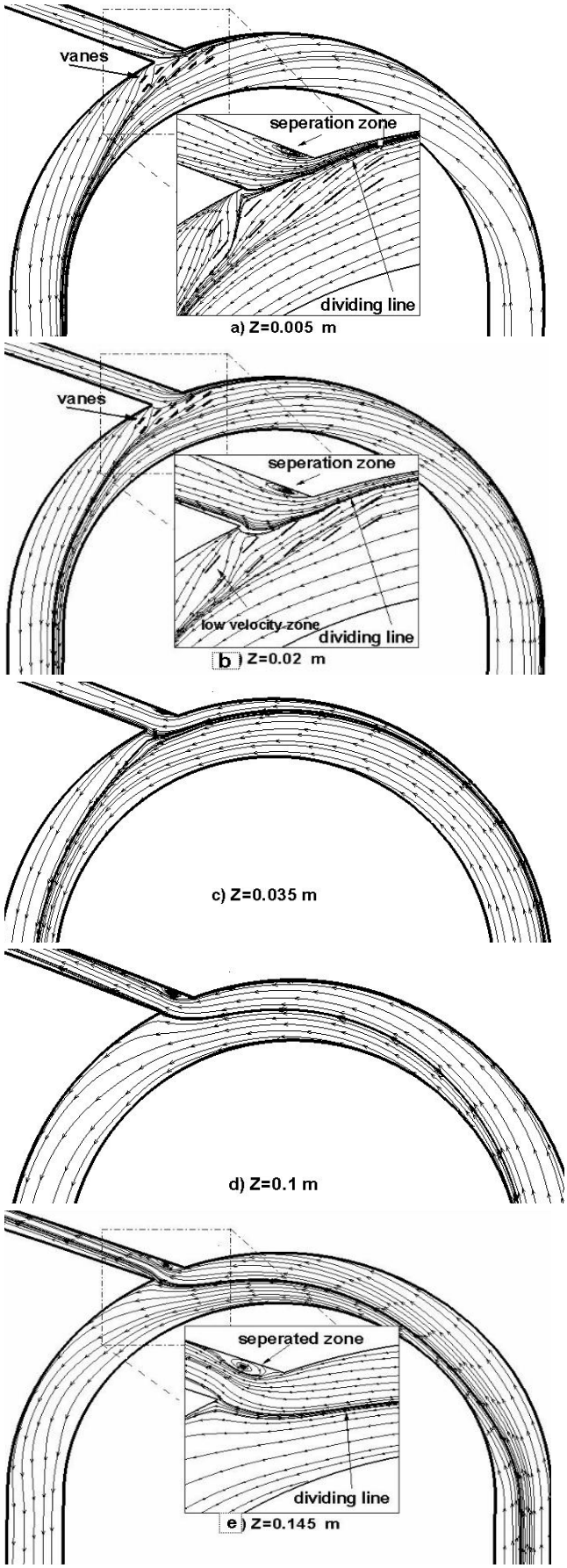

Figure 8: 2-D streamlines plots

strength of it decreases slowly up to the first vane position. When the flow attack vanes, the vane-induced secondary flow intensify it, but in front of the intake the intake secondary flow weaken it. After the intake, the strength of secondary flow tends to decrease.

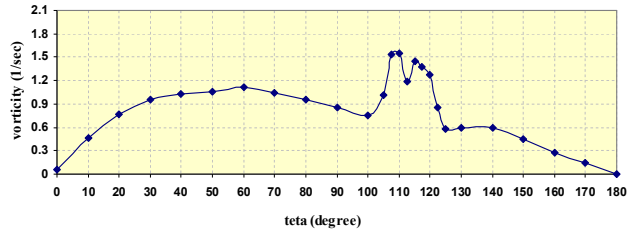

Figure 9: Strength of secondary flow

Conclusions

The CFD solver FLUENT is used to simulate the flow pattern around vanes placed in front of intake at 180° bend. Simulation performs well in estimating the velocity distribution and water surface profile with reasonable accuracy compared with experimental results. Flow pattern around vanes consists of a secondary flow at the same direction of the main secondary flow that intensifies it and overcome the intake secondary flow. The near bed contraction of the dividing stream surface by vanes reduces the proportion of the diversion flow from near bed. The implication of these flow patterns on sediment transport is that, more water is diverted with less amount of sediment for the branch channel.

References

Barkdoll, D., Ettema, R., & Odgaard, A. J. (1999). Sediment control at lateral diversions: limits and enhancement to vane use. *Journal of Hydraulic Engineering*, 125(8), pp. 132-136.

Daily, J. W., & Harleman, R. F. (1966). *Fluid dynamics*, Addishing-Westley Publishing Company.

Fluent Inc. (2005). *Fluent User' s Guide.*

Leschziner, M., & Rodi, W. (1979). Calculation of strongly curved open channel flow. *Journal of the Hydraulic Division*, 105(HY10), pp. 1299-1314.

Marelius, F., & Sinha, K. (1998). Experimental investigation of flow past submerged vanes. *Journal of Hydraulic Engineering*, 124(5), pp. 542-546.

Meselhe, E., & Sotiropoulos, F. (2003). Three-dimensional numerical model for open-channels with free-surface variations. *IAHR Journal of Hydraulic Research*. 41 (1), pp. 107-113.

Montaseri, H. (2007). *Effect of different arrangement of vanes on sediment control at water intakes at 180° bend.* PhD dissertation, Tarbiat Modares University, Tehran, Iran (in persian).

Neary, V.S., Sotiropoulos, F., & Odgaard, A. J. (1999). Three-dimensional numerical model of lateral-intake inflows. *Journal of Hydraulic Engineering*, 125(2), pp. 126-140.

Rostamabadi, M. (2007). Numerical Simulation of flow pattern around submerged vanes at 180 degree bend with intake. M Sc thesis, Tarbiat Modares University, Tehran, Iran (in persian).

Sinha, K. and Marelius, F. (2000). Analysis of flow past submerged vanes. *Journal of Hydraulic Research*, 38(1), pp. 65-71.

Soon-Keat, T., Guoliang, Y., Siow-Yong, L., & Muk-Chen, O. (2005). Flow structure and sediment motion around submerged vanes in open

channel. *Journal of Waterway, Port, Coastal and Ocean Engineering*, *ASCE*, 131(3), pp. 132-136.

Tarek, M., & Imran, J. (2004). Numerical modeling of three-dimensional flow field around circular piers. *Journal of Hydraulic Engineering*, 130(2), pp. 91-100.

Voisin, A., & Townsend, R. D. (2002). Model testing of submerged vanes in strongly curved narrow channel bends. *Journal of Civil Engineering*, 29, pp. 37-49

Wang, y., Odgaard, A. J., Melville, B. W., & Jain, S. C. (1996). Sediment control at water intakes. *Journal of Hydraulic Engineering*, 122(6), pp. .353-356.